5th Flow Control Conference
28 June - 1 July 2010, Chicago, Illinois

AIAA 2010-4841

Retrospective Cost Adaptive Control of Low-Reynolds Number Aerodynamics Using a Dielectric Barrier Discharge Actuator

Young-Chang Cho*, Jesse B. Hoagg†, Dennis S. Bernstein‡, and Wei Shyy§
Department of Aerospace Engineering, The University of Michigan, Ann Arbor, MI, 48109

The performance of micro air vehicles (MAVs) is sensitive to flow unsteadiness such as wind gusts, due to their low flight speed and light weight. We investigate the interplay of active flow control and stable flight performance. Specifically, a dielectric barrier discharge (DBD) actuator, characterized by fast response and non-moving parts, is used to control unsteady aerodynamics under fluctuating free-stream conditions on finite and infinite wings with the SD7003 airfoil geometry at chord Reynolds numbers between 300 and 1000. Feedback control is achieved using a retrospective cost adaptive controller, which adjusts control gains by minimizing a quadratic function of the retrospective performance and requires knowledge of nonminimum-phase (NMP) zeros (i.e., the complex numbers with magnitude greater than one where the transfer function equals zero) of the linearized flow-actuator model. The linearized flow-actuator system with lift as the performance has one real NMP zero, which approaches one as the distance between the actuator and the leading edge, Reynolds number, wing aspect ratio, or voltage increment decreases. At 15° angle-of-attack under modest free-stream fluctuation, DBD actuator commanded by the control law can stabilize lift by adjusting pressure and suction regions on the airfoil surface.

Nomenclature

AR	=	aspect ratio of a wing ($=b/c$)
b	=	span of a wing, m
c	=	chord length of a wing, m
C_D or C_d	=	drag coefficient of a wing or wing section
C_L or C_l	=	lift coefficient of a wing or wing section
C_p	=	pressure coefficient
$\mathbf{E}$ or E_i	=	electric field vector, N/C
$\mathbf{F}_b$ or F_{bi}	=	quasi-steady body force generated by the DBD actuator, N/m^3
H_i	=	i-th Markov parameter, 1/V
n_c	=	order of the controller
Re	=	Reynolds number
U_∞	=	free-stream speed, m/s
t^*	=	normalized time in the flow simulation ($=U_\infty t/c$)
V_{app}	=	voltage applied to the DBD actuator, kV

* Ph.D. Candidate, AIAA Student Member.
† Postdoctoral Research Fellow, AIAA Member.
‡ Professor, AIAA Member.
§ Clarence L "Kelly" Johnson Professor, AIAA Fellow.

$V_{app,0}$ = nominal voltage applied to the DBD actuator, kV

x_{act} = distance to the peak body-force of the DBD actuator from the airfoil leading edge, m

z_{NMP} = nonminimum-phase zero location

α = angle of attack of a wing, degree

α_d = vertical disturbance amplitude (flow speed ratio of maximum disturbance and vertical free-stream)

I. Introduction

THE performance of low-Reynolds-number flyers, specifically flyers with Reynolds numbers less than 10^5, is significantly affected by flow conditions[1]. Unlike higher-Reynolds-number flows, the flow structure in the low-Reynolds-number regime is sensitive to flow separation, laminar-turbulent transition, and flow reattachment[2]. Thus, the flight performance under unsteady ambient wind conditions is a major design issue[3,4]. Flow control at low Reynolds numbers involves free stream turbulence and flow unsteadiness, which may include changes in the transition point and the size of laminar separation bubble. Furthermore, at high angles of attack, the instability in a separated flow region induces unsteady vortex evolution, resulting in time-varying performance. The goal of low-Reynolds-number flow control is to decrease the laminar separation bubble, promote flow reattachment, and suppress vortex structure evolutions.

A dielectric barrier discharge (DBD), which is a gas discharge with a dielectric insulator, is known to generate neutral fluid flow under atmospheric pressure if the appropriate geometry and voltage waveform are used[5]. A DBD actuator does not require components for mass injection or mechanical moving parts. A DBD actuator can be easily installed on an airfoil due to the simple structure (i.e., electrodes divided by a thin dielectric insulator). DBD actuators are known to generate a thin layer of wall jet by delivering momentum to the neutral flow field from non-thermal ionized particles using a high intensity electric field[6]. Due to its high bandwidth (up to several kHz), this actuator can be a versatile control device for various applications. In addition, the duty cycle − the time duration that the actuator is turned on − as well as the amplitude of the applied voltage can be modulated to accommodate performance and power requirements.

Closed-loop active flow control can be used to achieve desired aerodynamic performance[7] and eliminate the influence of disturbances. For example, in Ref. 8 a linear quadratic regulator is used to stabilize the unstable states of a reduced order model constructed using the proper orthogonal decomposition technique. However, the flow dynamics at low Reynolds numbers vary significantly depending on flow conditions, making fixed-gain control difficult. Adaptive control techniques have the advantage of tuning the feedback gains in response to the true plant dynamics and exogenous signals. Nevertheless, these techniques typically require some model information, for example, reduced order models[9] or time-series models[10], and identifying this model information from high-dimensional flow fields can be challenging. More information about identifying time-series flow models can be found in Ref. 11 and Ref. 12.

In previous work[10], the retrospective cost adaptive control (RCAC) algorithm was applied to control the pressure drag of the SD 7003 airfoil at a Reynolds number of 300. RCAC updates the control parameters based on the retrospective performance, which is a surrogate measure of the true performance. RCAC requires limited model information, specifically, the delay, first nonzero Markov parameter, and nonminimum-phase (NMP) zeros of the linearized transfer function from the control to the performance. Furthermore, this model information can be estimated from the linearized system's Markov parameters, which are the impulse response coefficients of a discrete-time linear system. In particular, the NMP zeros can be estimated from the roots of a polynomial whose coefficients are constructed from a finite number of Markov parameters. Alternatively, the NMP zeros can be estimated by applying tailored system identification techniques[13]. Using Markov parameters is a convenient way of obtaining the required model information because in many cases they can be easily identified. For the flow-actuator system with a steady nominal state, the Markov parameters can be estimated by an open-loop impulse test.

Time delay and NMP zeros are known to restrict achievable performance of feedback control[14] and achievable bandwidth[15]. Specifically, the upper bound of the bandwidth is shown to decrease with increasing time delay or decreasing NMP zeros. Moreover, the delay and NMP zeros are dynamic characteristics that depend on the input-output behavior of a system, and cannot be modified by feedback control. The choice of measurements (i.e., the location and number of sensors) as well as actuators (i.e., the number and location of actuators) are important factors in determining the delay and zeros of a system, and thus, the achievable performance. In the current study, the single-input-single-output (SISO) control system is purposed where the aerodynamic lift is measured as the

performance variable. However, the response of the aerodynamic drag is also studied for the fluid dynamics perspective.

Numerical approaches to unsteady fluid dynamics require sufficient spatial and time resolutions in discretization to capture relevant flow structures and unsteady dynamics. For low-Reynolds-number applications of DBD actuators, the difference in both spatial and time scales between plasma operation and neutral flow evolution is large enough to use a quasi-steady assumption for the plasma dynamics. However, using a digital controller with the flow-actuator system introduces another time scale. Furthermore, if the data sampling or updating rate is changed, the dynamic system observed by the controller will change.

Using DBD actuation for adaptive flow control involves further issues, such as the impact of flow and actuator conditions on the system dynamics and control authority. For example, the actuator location affects not only static aerodynamic forces but also the dynamic force evolution. From a fluid dynamics perspective, it is important to understand the dynamic flow mechanisms that stabilize flow unsteadiness. Moreover, assessing the sensitivity of control performance, such as controllable fluctuations of aerodynamic forces, to actuator and control parameters is required, considering the limited power of DBD actuators.

Linear control theory has been applied to some nonlinear problems, for example flow control with linearized fluid equations[16] and electrical circuits with piecewise-linear model order reduction[17]. However, many fluid dynamics problems are highly nonlinear, especially low-Reynolds number airfoil flows, which often include flow separation and instabilities depending on flow conditions. This study demonstrates that flow conditions, such as Reynolds number and angle of attack, can significantly affect the linearized model of a fluid dynamic system. Furthermore, DBD actuation also affects the system dynamics and can excite the fluid dynamic system beyond the local linear regime. Note that such changes in flow conditions and the resulting nonlinearities may become too significant for many feedback control laws. Although the adaptive controller used in this study is nonlinear and capable of adjusting control gains, incorporating parametric changes of small time scales may not be feasible, even with online system identification. One of the key issues in the current flow control framework is the allowed parametric changes in achieving control goals such as stabilizing lift under a certain level of flow unsteadiness.

In this study, the response of the flow field to the DBD actuation and free-stream unsteadiness is investigated by identifying system parameters and stabilizing aerodynamic lift using the retrospective cost adaptive control algorithm. The flow-actuator system is a finite or infinite wing at the chord Reynolds numbers between 300 and 1000 and a DBD actuator on the upper surface of the wing. The angle of attack of the wing is 15°, which results in massive flow separation for the Reynolds number range of interest. In addition, a sinusoidal unsteadiness in vertical free-stream speed is introduced. The system parameters required for the controller, specifically the first nonzero Markov parameter and NMP zeros are estimated under different flow and actuation conditions − Reynolds number $Re = 300 \sim 1000$, wing aspect ratio $AR = 4 \sim \infty$, and actuation location $x_{act} = 0.05c \sim 0.7c$. For moderate disturbance magnitudes of $\alpha_d = 0.01 \sim 0.06$, the lift fluctuation is stabilized by feedback control, and the disturbance rejection mechanism of the DBD actuation is studied by exploring the flow field. Furthermore, the variations in the system parameters, which can occur at high levels of flow unsteadiness and restrict control performance, are explored along with the relevant flow physics.

II. Aerodynamics and DBD Actuator Models

A. Fluid Dynamics Model

The flow fields are analyzed by solving the incompressible Navier-Stokes equations using Loci-STREAM[18], a parallelized pressure-based unstructured finite volume code. Since the ion and electron states are non-equilibrium and the ion temperature is comparable to the neutral fluid, the neutral fluid is treated as being isothermal. Considering the time scale disparity between the low-Reynolds number flow and the radio frequency (RF) gas discharge of the DBD actuator, the force acting on the neutral fluid is assumed to be a quasi-steady body force. The body force felt by the neutral flow is equivalent to the Lorentz force acting on the net charge density. For the unsteady operation of the actuator only the amplitude variation of the operation voltage with time scales much larger than the RF operation is considered. In index notation, the relevant conservation equations are, for $i, j = 1, 2, 3$,

$$\frac{\partial u_j}{\partial x_j} = 0, \tag{1}$$

$$\frac{\partial u_i}{\partial t}+\frac{\partial\left(u_i u_j\right)}{\partial x_j}=\frac{F_{bi}}{\rho}-\frac{1}{\rho}\frac{\partial p}{\partial x_i}+\nu\frac{\partial}{\partial x_j}\left(\frac{\partial u_i}{\partial x_j}\right), \tag{2}$$

where, F_{bi} is DBD body force vector defined below. Here, x_i is Cartesian position in the global coordinate system, u_i is the flow velocity, ρ is the density, p is the pressure, ν is the kinematic viscosity of air.

B. DBD Actuator Model

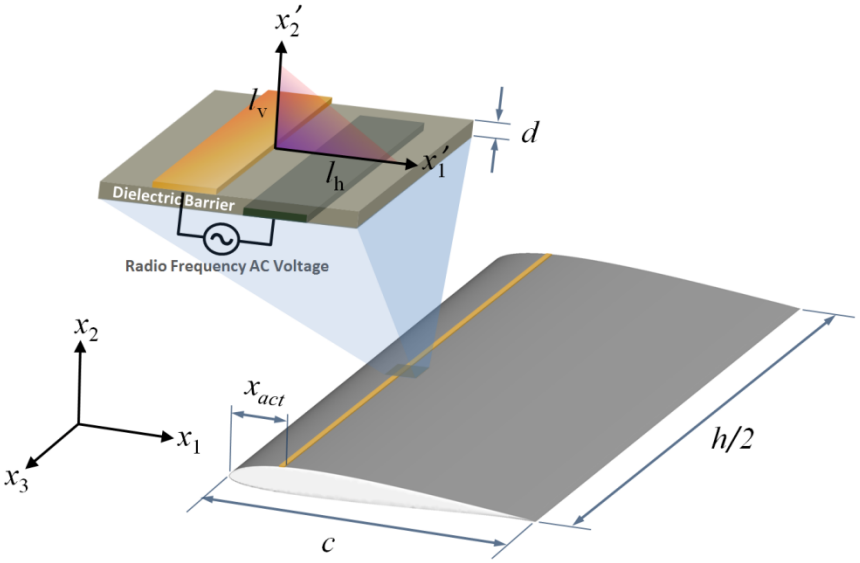

Figure 1 Schematics of wing and DBD actuator model.

The DBD actuator is modeled with linear electric field and constant net charge density[19]. As shown in Fig. 1, this model prescribes localized body forces in a triangular plasma region bounded by two electrodes and the dielectric surface. The electric field distribution inside the plasma region is approximated by spatially linear relations

$$\mathbf{E}'\left(x_1',x_2',t\right)=\left(\frac{\left|\mathbf{E}'\left(x_1',x_2',t\right)\right|k_2}{\sqrt{k_1^2+k_2^2}},\ \frac{\left|\mathbf{E}'\left(x_1',x_2',t\right)\right|k_1}{\sqrt{k_1^2+k_2^2}},\ 0\right), \tag{3}$$

where

$$\left|\mathbf{E}'\left(x_1',x_2',t\right)\right|=E_0\left(t\right)-k_1x_1'-k_2x_2',\quad E_0\left(t\right)=\frac{V_{app}\left(t\right)}{d}, \tag{4}$$

and (x_1',x_2') is the actuator local coordinate system, d is the insulator thickness, and k_1 and k_2 are the linearized slopes of the electric field in the x_1' and x_2' directions, respectively. This is a solution of Gauss' equation with the constant net charge density assumption. In (4), the maximum electric field intensity $E_0(t)$ is defined using the applied voltage and insulator thickness. The slopes k_1 and k_2 of the electric field attenuation away from the exposed electrode and dielectric surface are set to allow the breakdown voltage at the boundary with the minimum electric field strength. As shown in Ref. 19, this analytical-empirical model results in a body force component acting on the fluid, which is given by

$$\mathbf{F}_b\left(x_1,x_2,t\right)=\rho_c q_c\delta\left(x_1,x_2\right)f_v\Delta t_d\mathbf{E}\left(x_1,x_2,t\right), \tag{5}$$

where f_v is the AC frequency of the voltage applied to the DBD actuator, Δt_d is the discharge duty cycle, and $\mathbf{E}(x_1,x_2,t)$ is the electric field distribution (3) transformed to the global coordinate system. Furthermore, since the constant charge density ρ_c with unit charge q_c is present only inside the plasma region, $\delta(x_1,x_2)$ is set to 0 or 1 depending on the position. The plasma region is invariant along x_3-axis on the wing. For this study, the horizontal electric field length $l_h=0.05c$ and vertical length $l_v=0.025c$. The discharge duty cycle is the portion of time during which effective force generation occurs in each operation cycle. Under feedback control, the applied voltage to the electrode depends on the control signal, resulting in a time-varying body force. Since the reduced-order DBD

model (3) ~ (5) is based on the quasi-steady assumption using the time scale disparity, the control input is meaningful when its timescale lies between those of low Reynolds number flow and plasma operation. The DBD model has been validated against experimental data of force generation[20] and maximum induced flow velocity[21].

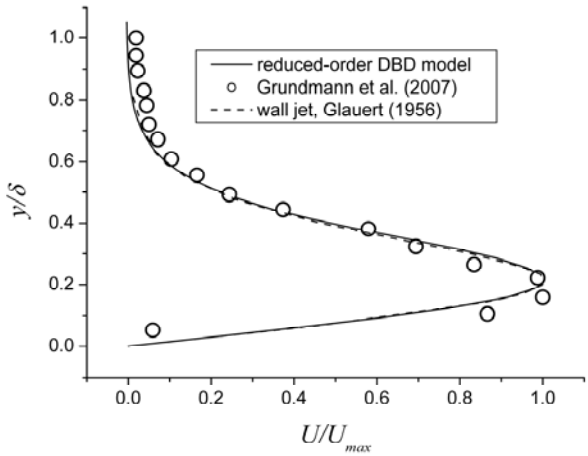

Figure 2 Velocity profile of the induced wall jet.

The velocity profile of the flow induced by the reduced-order DBD model is shown in Fig. 2, where U is the flow speed parallel to the wall, U_{max} is the maximum flow speed, y is the distance from the wall, and δ is the height where $U \simeq 0$. Since the flow downstream of the actuator is a momentum jet, the velocity profile is independent of the streamwise distance and consistent with the similarity solution in Ref. 22.

In order to assess the resultant performance of the DBD actuator and controller, a single co-flow directional DBD actuator with voltage amplitude modulation according to the control input is used in this study, and the position of the actuator is changed such as $x_{act}/c = 0.05 \sim 0.7$.

III. Control Algorithm

In this section, we summarize the adaptive control algorithm presented in Ref. 23 for a single-input, single-output control system. The details of the multi-input, multi-output algorithm are shown in Ref. 23. Consider the single-input, single-output linear discrete-time system

$$x(k+1) = Ax(k) + Bu(k) + D_1 w(k), \tag{6}$$

$$z(k) = E_1 x(k) + E_0 w(k), \tag{7}$$

where $x(k) \in \mathbb{R}^n$, $\mathrm{z}(k) \in \mathbb{R}$, $\mathrm{u}(k) \in \mathbb{R}$, $\mathrm{w}(k) \in \mathbb{R}^{l_w}$ are the state, performance, control, and exogenous command and/or disturbance signal with $k \geq 0$. We present an adaptive output feedback controller under which the performance variable z is minimized in the presence of the exogenous signal w, which could be a disturbance, command, or both. In this paper, we use an adaptive feedback controller to minimize the variation of the aerodynamic lift acting on the airfoil under inlet flow conditions with a sinusoidal disturbance.

For the general control problem given by (6)-(7), we use a strictly proper time-series controller of order n_c, such that the control $u(k)$ is given by

$$u(k) = \sum_{i=1}^{n_c} M_i(k) u(k-i) + \sum_{i=1}^{n_c} N_i(k) z(k-i), \tag{8}$$

where, for all $i = 1, \cdots, n_c$, $M_i(k)$, $\mathrm{N}_i(k) \in \mathbb{R}$ are given by the adaptive law presented below. The control can be expressed as

$$u(k) = \theta^T(k) \phi(k), \tag{9}$$

where

$$\theta(k) \triangleq \begin{bmatrix} N_1(k) & \cdots & N_{n_c}(k) & M_1(k) & \cdots & M_{n_c}(k) \end{bmatrix}^T \in \mathbb{R}^{2n_c} \tag{10}$$

is the controller parameter matrix, and the regressor vector $\phi(k)$ is given by

$$\phi(k) \triangleq \begin{bmatrix} z(k-1) \\ \vdots \\ z(k-n_c) \\ u(k-1) \\ \vdots \\ u(k-n_c) \end{bmatrix} \in \mathbb{R}^{2n_c} \tag{11}$$

For positive integer μ, we define the extended control vector $U(k)$ by

$$U(k) \triangleq \begin{bmatrix} u(k) \\ \vdots \\ u(k-p_c+1) \end{bmatrix} \in \mathbb{R}^{p_c} \tag{12}$$

where $p_c \triangleq \mu+1$. From (9), it follows that the extended control vector $U(k)$ can be written as

$$U(k) \triangleq \sum_{i=1}^{p_c} L_i \theta^T (k-i+1) \phi(k-i+1), \tag{13}$$

where

$$L_i \triangleq \begin{bmatrix} 0_{(i-1)\times 1} \\ 1 \\ 0_{(p_c-i)\times 1} \end{bmatrix} \in \mathbb{R}^{p_c}. \tag{14}$$

Next, define the retrospective performance

$$\hat{z}(\hat{\theta},k) \triangleq z(k) - \bar{B}_{zu}\left(U(k) - \hat{U}(\hat{\theta},k)\right), \tag{15}$$

where $\hat{U}(\hat{\theta},k) \triangleq \sum_{i=1}^{p_c} L_i \hat{\theta}^T \phi(k-i+1)$, $\hat{\theta} \in \mathbb{R}^{2n_c}$ is an optimization variable, and control matrix $\bar{B}_{zu}$ is given by (25) below. Note that $\hat{z}(\hat{\theta},k)$ is obtained by modifying the performance variable $z(k)$ based on the difference between the actual past control inputs $U(k)$ and the recomputed past control inputs $\hat{U}(\hat{\theta},k)$ assuming that $\hat{\theta}$ had been used in the past. Thus, $\hat{z}(\hat{\theta},k)$ may be interpreted as an approximation of the performance had $\hat{\theta}$ been used in the past.

Now, consider the retrospective cost function

$$\hat{J}(\hat{\theta},k) \triangleq \hat{z}^2(\hat{\theta},k) + \alpha_l(k)\left(\hat{\theta} - \theta(k)\right)^T \left(\hat{\theta} - \theta(k)\right), \tag{16}$$

where the learning rate $\alpha_l(k) \in \mathbb{R}$ affects the transient performance and the convergence speed of the adaptive control algorithm. Substituting (15) into (16) yields

$$\hat{J}(\hat{\theta},k) = \hat{\theta}^T A(k) \hat{\theta} + b^T(k)\hat{\theta} + c(k), \tag{17}$$

where

$$A(k) \triangleq D^T(k)D(k) + \alpha_l(k) I_{2n_c}, \tag{18}$$

$$b(k) \triangleq 2D^T(k)\left(z(k) - \bar{B}_{zu}U(k)\right) - 2\alpha_l(k)\theta(k), \tag{19}$$

$$c(k) \triangleq \left(z(k) - \bar{B}_{zu}U(k)\right)^2 + \alpha_l(k)\theta^T(k)\theta(k), \tag{20}$$

and $D(k) \triangleq \bar{B}_{zu} \sum_{i=1}^{p_c} \left(L_i \phi^T(k-i+1)\right)$. Since $A(k)$ is positive definite, $\hat{J}(\hat{\theta},k)$ has the unique global minimizer $-\frac{1}{2}A^{-1}(k)b(k)$. Thus, the update law is given by

$$\theta(k+1) = -\frac{1}{2} A^{-1}(k) b(k). \tag{21}$$

The adaptive controller (9) and (18)-(21) requires limited model information of the plant (6)-(7); however, the controller does require knowledge of $\bar{B}_{zu}$. In this paper, we construct $\bar{B}_{zu}$ using estimates of the plant's relative degree, first nonzero Markov parameter, and the nonminimum-phase zeros of the transfer function from u to z. Consider the transfer function from u to z given by

$$G_{zu}(z) \triangleq E_1 (zI - A)^{-1} B, \tag{22}$$

which can be written as

$$G_{zu}(z) \triangleq H_d \frac{\beta(z)}{\alpha(z)}, \tag{23}$$

where the relative degree $d \geq 1$ is the smallest positive integer i such that the i-th Markov parameter $H_i \triangleq E_1 A^{i-1} B$ is nonzero, and $\alpha(z)$ and $\beta(z)$ are monic coprime polynomials. Next, let $\beta(z)$ have the factorization

$$\beta(z) = \beta_u(z) \beta_s(z), \tag{24}$$

where $\beta_s(z)$ is a monic polynomial of degree n_s whose roots lie inside the unit circle, and $\beta_u(z)$ is a monic polynomial of degree n_u whose roots lie on or outside the unit circle. Furthermore, we can write $\beta_u(z) = z^{n_u} + \beta_{u,1} z^{n_u - 1} + \cdots + \beta_{u,n_u - 1} z + \beta_{u,n_u}$. Then we let $\mu = n_u + d$ and the resulting control matrix $\bar{B}_{zu}$ is given by

$$\bar{B}_{zu} \triangleq H_d \begin{bmatrix} 0_{1\times d} & 1 & \beta_{u,1} & \cdots & \beta_{u,n_u} \end{bmatrix} \in \mathbb{R}^{1\times p_c}. \tag{25}$$

Note that $\bar{B}_{zu}$ is constructed using knowledge of the relative degree d, the first nonzero Markov parameter H_d, and the nonminimum-phase zeros of $\beta_u(z)$ of the transfer function from u to z. Other constructions of $\bar{B}_{zu}$ are shown in Ref. 24.

IV. Results and Discussion

A. Effect of DBD Actuation on High Angle of Attack Unsteady Flow

In this study, an angle of attack (α) of 15° is used to explore the dynamics of unsteady flow separation without actuation. An example flow structure around a finite wing with Re = 1000, based on the free-stream speed $U_\infty = \sqrt{U_1^2 + U_2^2 + U_3^2}$, where (U_1, U_2, U_3) is free-stream velocity, and wing chord c, is shown in Fig. 3. Without any disturbance in the free-stream flow, the separated flow is unstable and induces unsteadiness in the flow field. Specifically, Fig. 3 shows a periodic evolution of the vortex structures with a non-dimensional period of 1.61; the compact vortex pair causing maximum lift evolves to a single weak vortex generating minimum lift.

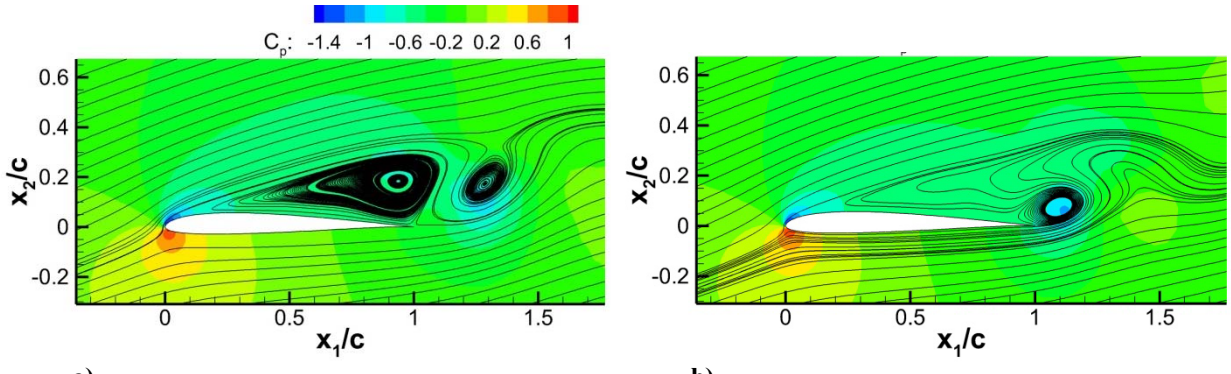

Figure 3 Streamlines and pressure contours without actuation (Re = 1000, α = 15°): a) maximum lift instant; b) minimum lift instant.

If there is a disturbance in the free-stream flow, for example in the vertical flow speed, the vortex instability in the separated flow region is coupled with the free-stream unsteadiness. In this case, the free-stream velocity is

$\mathbf{U}(t^*) = (U_1, U_2(1+\alpha_d \sin(2\pi t^*/T^*)), U_3)$, where $t^* = U_\infty t/c$ is the non-dimensional time, α_d is the disturbance amplitude, and T^* is the non-dimensional disturbance period. As shown in Fig. 4a, if the frequency difference between the instability of the separated flow and the free stream unsteadiness is large, the two time scales are separated. However, if the two time scales have the same order of magnitude (as shown in Fig. 4b), two fluctuations are coupled, resulting in larger amplitude variations in drag and lift even with the lower disturbance amplitude.

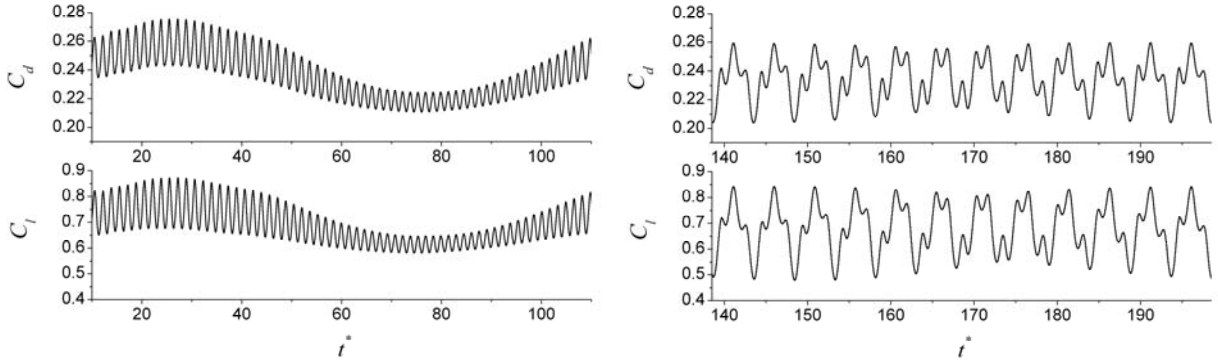

a) **b)**

Figure 4 drag and lift time histories with the sinusoidal disturbance in vertical free-stream speed (*Re* = 1000, $\alpha = 15^\circ$): a) $T^* = 100$, $\alpha_d = 0.1$; b) $T^* = 5$, $\alpha_d = 0.06$.

When the actuator is activated, the body-force field generates an induced flow near the airfoil surface as shown in Fig. 5a. The reduced-order DBD actuator model approximates the body-force field inside the ionized gas volume with quasi-steady linear distributions of positive x_1-directional and negative x_2-directional forces. The actuation V_{app} = 1 kV induces a maximum flow speed as the same order as the free-stream speed U_∞. For V_{app} = 1 kV, the maximum non-dimensional body force, normalized by the inertial force of the free stream condition, is approximately 97.2. While inducing the flow entrained from the surrounding air and accelerated to downstream, the actuator generates suction and pressure regions upstream and downstream of the actuation position, respectively. As a result of the induced wall jet, the additional wall shear stress contributes to drag increase. When this wall-jet is applied to the flow with α = 15°, the separated flow region is decreased and the unsteady separated region is stabilized with a reduced separated-flow region as shown in Fig. 5b.

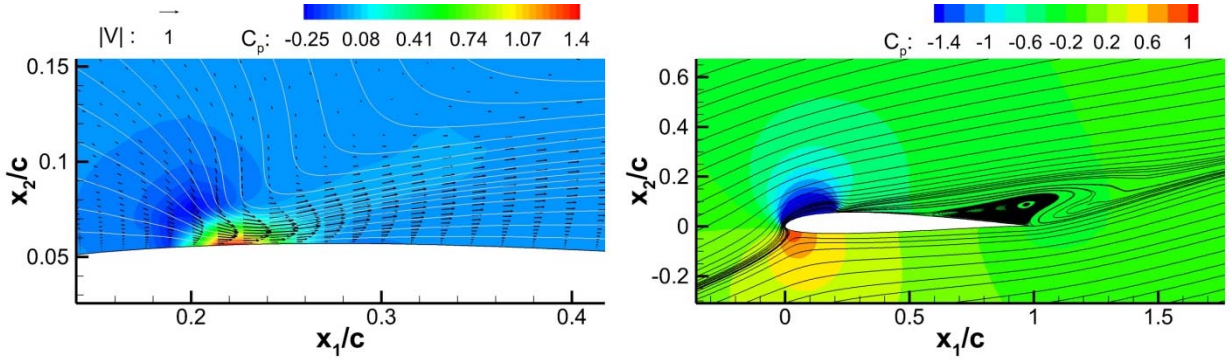

a) **b)**

Figure 5 Flow field with 1 kV actuation (actuator length: l_h/c= 0.05, position: x_{act}/c = 0.2): a) velocity vectors, streamlines and pressure contours without free-stream; b) streamlines and pressure contours with free-stream (*Re* = 1000, $\alpha = 15^\circ$).

B. Identification of the Flow-Actuator System

At each flow time step, the flow field is calculated, followed by the performance measurement and voltage update, provided that the flow time step coincides with the control time step. As a result, there is a system delay of at least 1 in the control time scale unit, regardless of the flow time resolution. Fig. 6a shows a typical impulse response of the aerodynamic lift and the Markov parameters (i.e., impulse response coefficients) estimated from the impulse response. Although the flow-actuator system is infinite dimensional, it is approximated with a linear discrete-time

model with the finite number of Markov parameters around a nominal actuation condition. The order of the linear system can be estimated by the number of dominant singular values of the block-Hankel matrix, which is a square block matrix whose skew diagonal matrices are composed of the Markov parameters from $H_0 \sim H_{2n-2}$, where n is the order of the system. For example, the estimated order of the system shown in Fig. 6b is approximately 6. For the conditions tested in this study the order is less than 10, and no noticeable difference in the system order is observed between Re = 300 and 1000. On the other hand, the order increases as the flow time resolution increases. As shown in section D, however, capturing higher frequency responses is not necessarily beneficial for the current examples. In addition, the current flow time resolution is shown to be sufficient to represent the dynamics of the flow-actuator system.

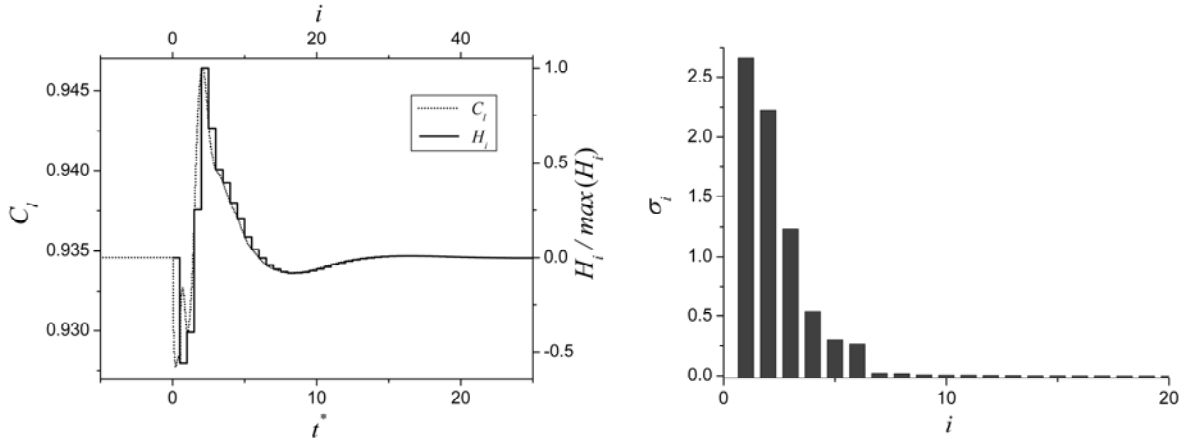

a) **b)**

Figure 6 Impulse response and system identification for lift (Re = 1000, α = 15°, $V_{app,0}$ = 1 kV, ΔV_{app} = 0.2 kV, H_i: i-th Markov parameter, σ_i: i-th singular value): a) impulse response and identified Markov parameters; b) singular values of the block-Hankel matrix.

The estimated Markov parameters include the information of system zeros. More specifically, some of the roots of the Markov parameter polynomial approximate the zeros that lie outside of the unit circle in the complex domain; these are the nonminimum-phase (NMP) zeros or unstable zeros of the linearized transfer function. As opposed to the drag response where no NMP zero is observed in most cases, thus the linearized transfer function from the control to drag is minimum-phase, the one from the control input to lift is NMP, mostly with one real NMP zero in the current study. This difference can be attributed to the fluid dynamics under the influence of the DBD actuation.

The step response of a system with an odd number of NMP zeros has initial undershoot, that is, the step response initial move in the direction opposite to its steady-state value[25]. For example, the step response of a system with one real NMP zero, having positive steady-state output, initially decreases then increases to reach the steady-state value. A system with multiple NMP zeros repeats the step response with ripples which cross the undisturbed value as many times as the number of real NMP zeros before reaching the steady-state output. Moreover, for a continuous-time system, the relative undershoot r_y, that is the ratio of the undershoot amplitude and the steady-state value in a step response, is known to decrease as the NMP zero increases[26,27]. By relating the NMP zero and dynamic response of a system, the relative undershoot is informative to understand the relative NMP zero positions of a system under different conditions. For example, the increased undershoot or decreased steady-state value means a smaller NMP zero as well as a larger relative undershoot.

As noted earlier, the impact of the DBD actuation on the flow field under the flow and actuator conditions can be summarized as the intensified suction and pressure peaks around the actuation position, increased wall shear stress and reduction of flow separation. At these low Reynolds numbers, the drag reduction due to the reduced separation region by the induced wall jet is less than the drag increase due to the viscous forces, resulting in the increase of the steady-state drag with actuation. Moreover, at the moment of actuation, the induced jet increases the local viscous drag before affecting the separated flow region. As a result, the impulse actuation increases drag without undershoot, and the system for drag is either minimum phase or NMP with an even number of NMP zeros. For the flow and actuator conditions in this study, the system with drag as the performance is estimated to be minimum-phase or NMP with an even number of complex NMP zeros. Lift, on the other hand, initially decreases due to the downward

flow induced by the negative x_2-directional body force field but then increases due to the intensified suction and the enhanced pressure recovery by the reduced flow separation, resulting in the step response with initial undershoot. It is consistent with this observation that the impulse response tests for lift show one real NMP zero. Since the initial impact of the actuation on aerodynamic forces determines whether the system has initial undershoot in the step response or not, the local variations of pressure and viscous force fields caused by the DBD actuation are major factors affecting the difference between systems with lift and drag as the performance.

C. Disturbance Rejection with Feedback Control

Assuming no information about the flow unsteadiness is known *a priori*, the retrospective adaptive controller is applied to the feedback loop to eliminate the impact of the flow unsteadiness. The ratio of control and flow time steps is set to 10 to limit the bandwidth of the control system. We use the zero-order-data hold[28], which keeps the control constant between control time steps. The sensitivity of control performance on the time step ratio is discussed in section D.

Fig. 7 shows feedback control results for sinusoidal disturbances in the vertical free-stream speed with different disturbance magnitudes and frequencies. The objective is to minimize the difference between the undisturbed lift with the nominal actuation and the measured lift under the influence of the disturbance. For both Fig. 7a and b, the impact of sinusoidal disturbances on the airfoil lift is suppressed by the DBD actuator with the time-varying voltage signal determined by the controller. The fluctuation of drag, on the other hand, is amplified for $T^* = 100$, while suppressed for $T^* = 10$, which implies the actuation can be beneficial in both lift and drag depending on the disturbance frequency.

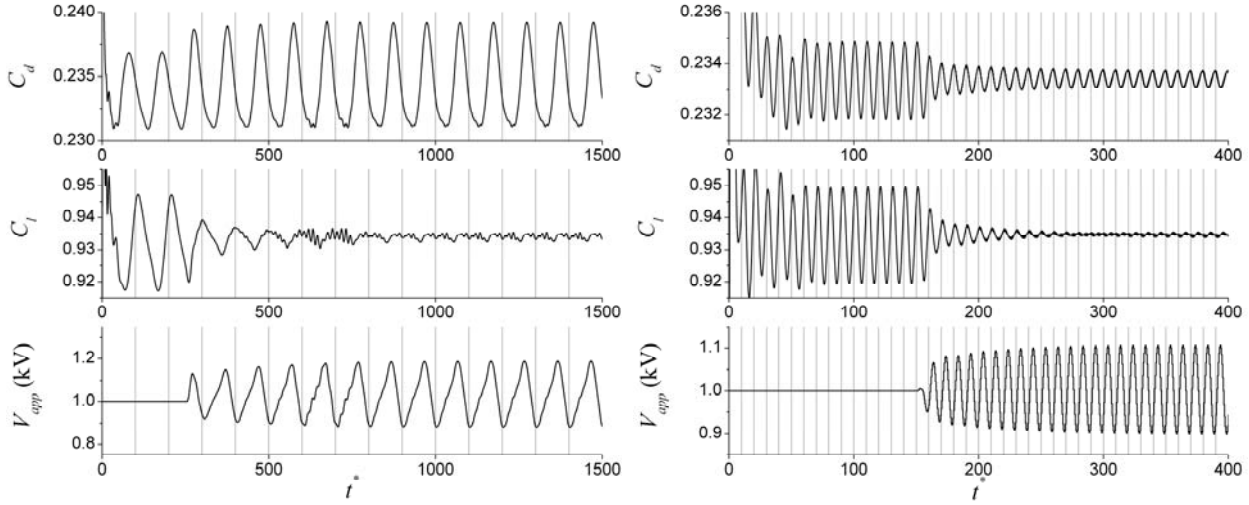

Figure 7 Feedback control result of aerodynamic forces and control input for disturbance rejection (Re = 1000, $AR = \infty$, $\alpha = 15^\circ$, $V_{app,0} = 1$ kV, learning rate = 200, $n_c = 50$, 3 system parameters capturing 1 NMP zero and delay): a) $T^* = 100$, $\alpha_d = 0.06$; b) $T^* = 10$, $\alpha_d = 0.01$.

The variation in vertical flow speed induces changes in both flow speed and angle of attack, and aerodynamic forces are also subject to the response of the separated flow to the changes. As shown in Fig. 7a, for the disturbance with a lower frequency and a higher amplitude, the phase difference between open-loop drag and lift fluctuations is larger than the one with a higher frequency and a lower amplitude in Fig. 7b. In addition, the closed-loop control voltage is close to the reverse of the lift variation for both cases, resulting in the suppression of the lift fluctuation. As a result, the control voltage signal of Fig. 7a is in phase with the drag fluctuation, amplifying the drag fluctuation. On the other hand, drag and lift are in phase with each other in Fig. 7b and the control voltage suppresses both drag and lift fluctuations.

For the case of Fig. 7a, streamlines and pressure contours under the open-loop (i.e., constant voltage) actuation are shown in Fig. 8a and b, when the lift is minimum and maximum, respectively. Since the amplitude of the closed-loop voltage variations is too small to cause a noticeable difference in the flow structure, Fig. 8a and b also correspond the phases when the closed-loop control voltage is maximum and minimum, respectively. The distribution shown with the dotted line is the local pressure difference between the closed-loop and open-loop

actuations at each phase. The sections with dotted lines inside and outside the airfoil geometry denote the regions where the voltage change causes pressure increase and pressure decrease, respectively.

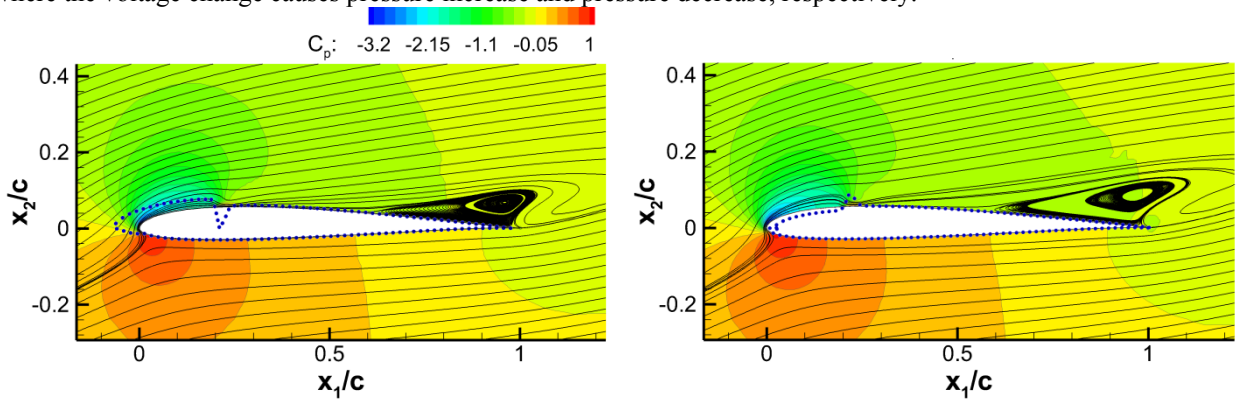

a) b)

Figure 8 Streamlines and pressure contours with 1 kV actuation, and compensated pressure distribution under feedback control (Re = 1000, $AR = \infty$, $\alpha = 15^{\circ}$, $T^* = 100$, $\alpha_d = 0.06$, $V_{app,0} = 1$ kV, $x_{act}/c = 0.2$): a) minimum lift (maximum voltage); b) maximum lift (minimum voltage).

Since the jet induced by the actuator is almost horizontal and the viscous force augmented by the actuation hardly contributes to lift as a result, the variation in pressure distribution mostly contributes to the lift variation. Although the closed-loop voltage variation is not large enough to resize the separated flow structure, the relative pressure distributions suggest the lift stabilization mechanism. At the instant of minimum lift, the controller increases the actuation voltage, intensifying the suction pressure near the leading edge as shown in Fig. 8a. Though the pressure distributions downstream of the actuator and downside of the wing are hardly changed, the net pressure change near the leading edge and the actuator contributes to enhancing lift. When the disturbance causes maximum lift, on the other hand, the controller decreases the voltage, reducing suction and pressure peaks as shown in Fig. 8b to mitigate the lift increase.

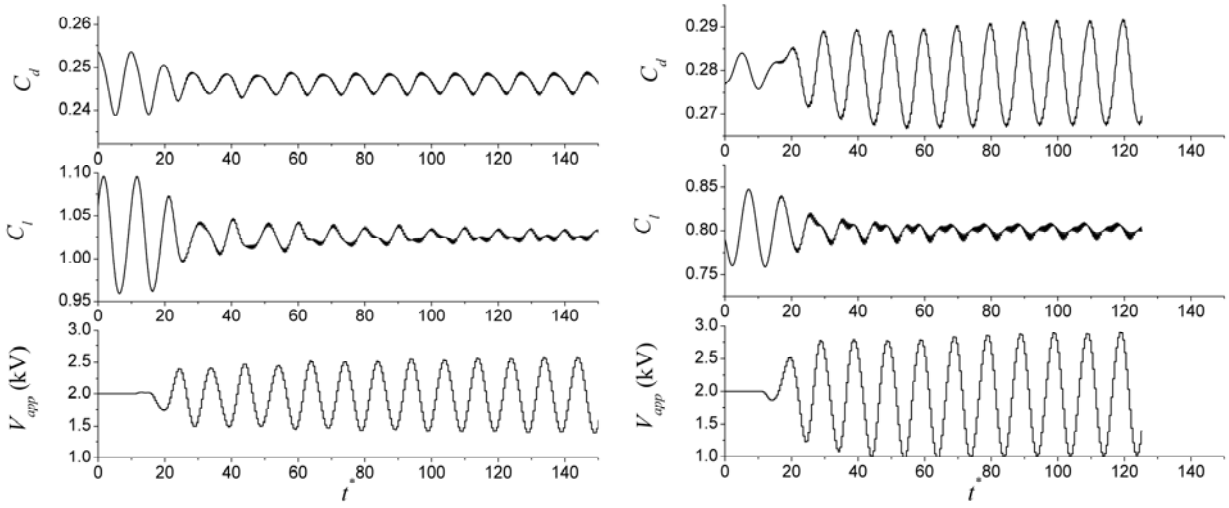

a) b)

Figure 9 Feedback control result of aerodynamic forces and control input for disturbance rejection (Re = 1000, $\alpha = 15^{\circ}$, $T^* = 10$, $\alpha_d = 0.05$, $V_{app,0} = 2$ kV, learning rate = 300, $n_c = 50$, 3 system parameters capturing 1 NMP zero and delay): a) $AR = \infty$; b) $AR = 4$.

The control performances for different wing aspect ratios are compared in Fig. 9. Compared to the infinite wing, the higher voltage variation is required for the finite wing, implying that the control authority on lift is decreased. Even with the same disturbance, there are phase differences in force responses between infinite and finite wings, and drag fluctuation is increased by stabilizing lift for the finite wing, as opposed to the reduced drag fluctuation for the

infinite wing. It is observed that the control authority on lift decreases and penalty for drag increases, as the wing aspect ratio decreases.

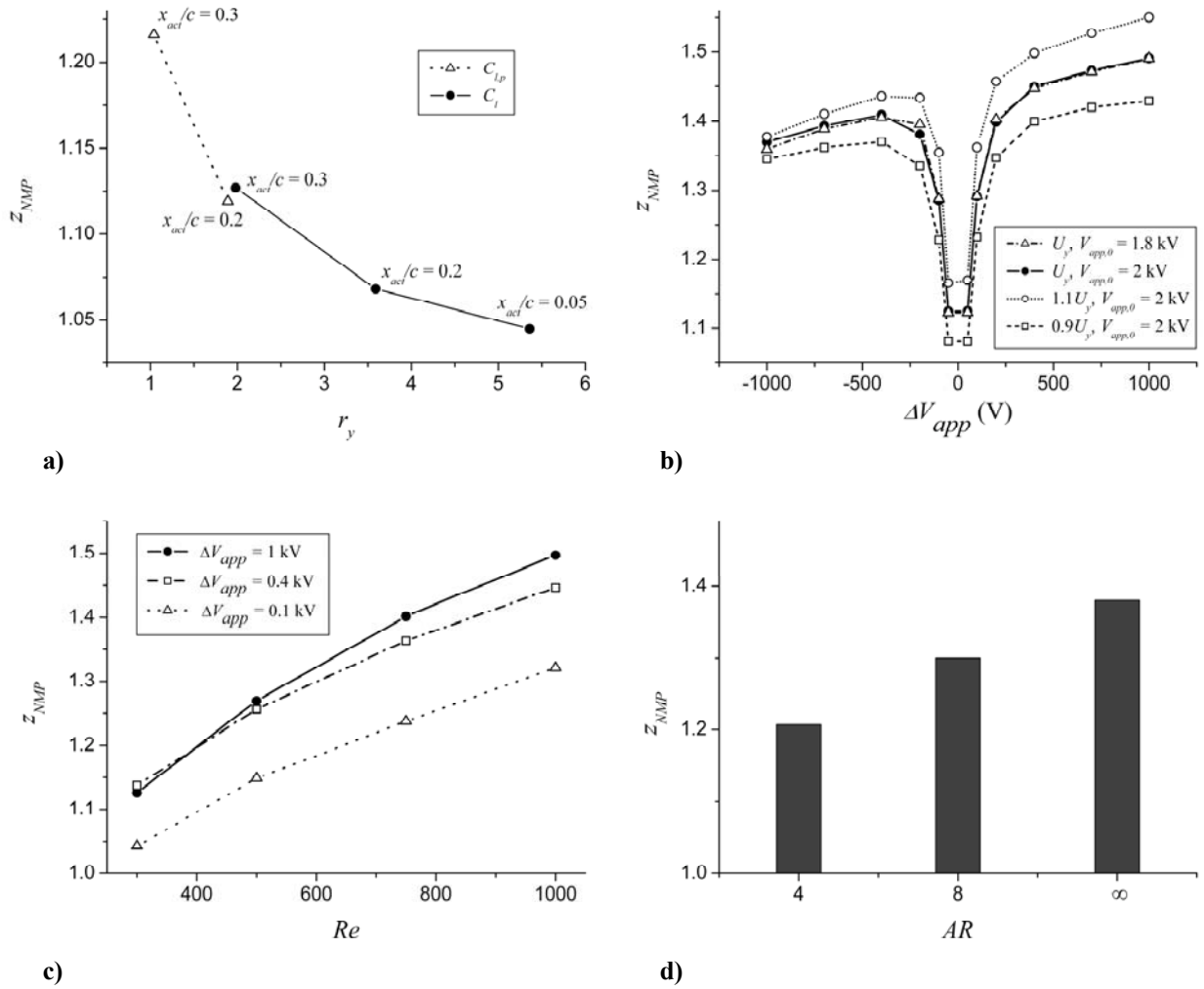

Figure 10 Geometric, flow and actuation conditions, and the real NMP zero for lift: a) relative undershoot r_y and NMP zero with actuation location (Re = 300, $V_{app,0}$ = 1 kV, ΔV_{app} = 3 kV, $C_{l,p}$: pressure lift coefficient); b) impulse amplitude and NMP zero with nominal voltage and vertical free-stream speed (Re = 1000, x_{act}/c = 0.2); c) Reynolds number and NMP zero with impulse amplitude (x_{act}/c = 0.2, $V_{app,0}$ = 1 kV); d) wing aspect ratio and NMP zero (Re = 1000, x_{act}/c = 0.2, $V_{app,0}$ = 2 kV, ΔV_{app} = 1 kV).

D. Drift of System Parameters

For the test cases, the identified system parameters, or more specifically the first nonzero Markov parameter and real NMP zero, are dependent on the flow and actuator conditions. The relevant questions can be summarized as the following. How much do the system parameters change according to the flow and actuation conditions, and actuation itself? How accurately the system parameters should be estimated or how much tolerance to their changes does the control system have? Is it possible to minimize or incorporate the parametric changes with the control algorithm to achieve control goals? The nonlinearity caused by the parametric change can invalidate the linear model assumption on which the control algorithm based. Thus, assessing the parametric change helps to address the limitation of the current framework and suggest the direction to improve the control performance.

For a continuous-time system, since the real NMP zero value is inversely proportional to the relative undershoot as mentioned in section B, the change either in the undershoot magnitude or steady-state value in the lift step response indicates the variation of the real NMP zero; the NMP zero increases if either the undershoot amplitude decreases or the steady-state lift increases. The same trend is observed for the discrete-time flow-actuator system in this study. As an example, the relation between the relative undershoot and the real NMP zero in lift for Re = 300 is

shown in Fig. 10a for different actuation locations. For both pressure lift and total lift, the real NMP zero increases, as the actuation position moves downstream. Since the increase of the steady-state lift caused by the increase of x_{act}/c results in the decrease of the relative undershoot, the relation between the relative undershoot and real NMP zero is consistent with the one in continuous-time systems.

In this study it is also observed that the feedback performance is significantly affected by the disturbance period in the range of $T^* = 5 \sim 100$ and magnitude of the disturbance in vertical free-stream speed in the range of $\alpha_d = 1 \sim 6$ %. A higher disturbance magnitude changes system dynamics by changing both the instantaneous angle of attack and flow speed. Furthermore, the control voltage variation at each time step should be increased as the disturbance amplitude increases. As shown in Fig. 10b, the real NMP zero of lift is asymmetric with respect to the sign of the impulse voltage and decreases as the impulse magnitude approaches to 0. This NMP zero drift indicates the sensitivity of system parameters on voltage increment or disturbance magnitude. It is also shown that the change in vertical free-stream speed also induces the NMP zero drift.

In Fig. 10c, the variation of the real NMP zero according to the Reynolds number as well as the voltage increment is shown. As Reynolds number increases between $Re = 300$ and 1000, the real NMP zero becomes larger, which is analogous to the trend with the relative undershoot, considering the increase of the steady-state lift at higher Reynolds numbers. Though the undershoot magnitude increases as Reynolds number increases, which is shown in the following, the increase of the steady-state lift at a higher Reynolds number dominates the relative undershoot. The relation between the impulse magnitude and the real NMP zero is also influenced by the Reynolds number. The impact of the wing aspect ratio on the real NMP zero is shown in Fig. 10d and the trend can also consistent with the enhanced steady-state lift with a higher aspect ratio wing.

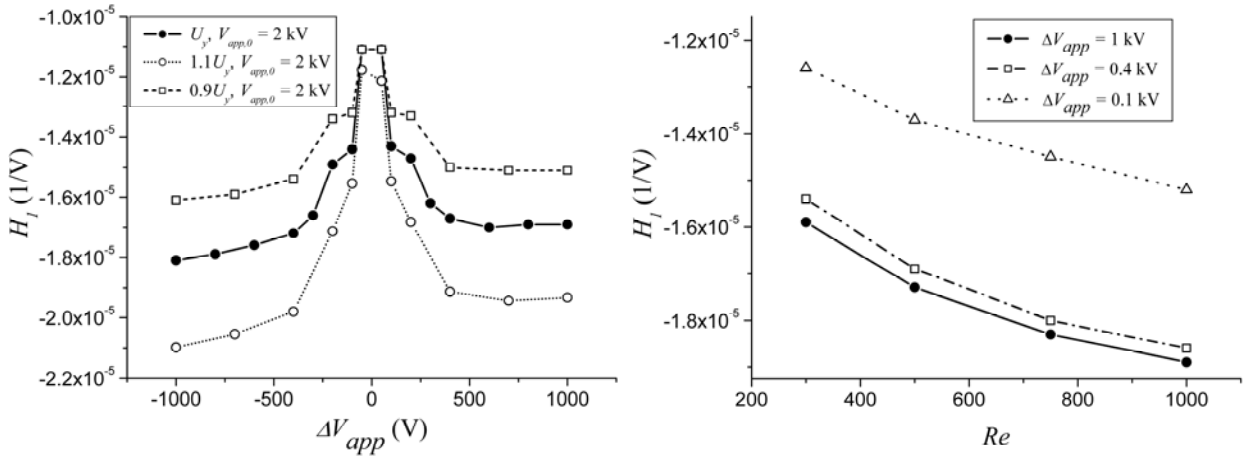

a) **b)**

Figure 11 Flow and actuation conditions, and the first nonzero Markov parameter: a) impulse amplitude and the first nonzero Markov parameter with vertical free-stream speed and nominal voltage ($Re = 1000$, $x_{act}/c = 0.2$); b) Reynolds number and the first nonzero Markov parameter with impulse amplitude ($x_{act}/c = 0.2$, $V_{app,0} = 1$ kV).

The first nonzero Markov parameter shown in Fig. 11 also depends on the flow and actuation conditions. The first nonzero Markov parameter indicates the fastest response of the aerodynamic lift to the actuation voltage. As discussed in section B, the parameter is negative for lift, and a higher free-stream speed, Reynolds number or voltage increment increases the absolute value of the first nonzero Markov parameter. As a result, the absolute value of the first nonzero Markov parameter has a trend similar to the real NMP zero.

As mentioned earlier, there exist flow and control time scales in the current flow control simulations. The non-dimensional time resolution of flow simulations in this study is $\Delta t_f^* = U_\infty \Delta t_f / c = 0.05$. Since the discontinuous voltage update at each control time step induces high-frequency input to the flow-actuator system, the flow time resolution should be sufficient to resolve flow dynamics critical in system parameters. In Fig. 12a, for example, the impulse responses with $\Delta t_f^* = 0.05$ (case A) and with $\Delta t_f^* = 0.01$ (case B) are compared, while keeping the control time resolution same. The transient oscillation between $t^* = 5$ and 12 is not captured with the coarser time resolution. However, the overall response (or system parameters) is consistent with each other, and the estimated real NMP zero

remains virtually same, implying the current flow time resolution is sufficient to capture key flow dynamics of the system.

The control time resolution, on the other hand, significantly affects the system parameters. For example, the comparison between $\Delta t_c^* = 0.5$ (case B) and $\Delta t_c^* = 0.1$ (case C) in Fig. 12a indicates that the smaller control time step not only causes a reduced impact of the impulse and resolves higher frequencies but also results in the noticeably different flow response. Moreover, as shown in Fig. 12b, the identified transfer function of the actuator-flow system with $\Delta t_c^* = 0.1$ (case C) shows three NMP zeros located close to the unit circle, as opposed to the one real NMP zero with the larger control time step. As a result, it is observed in this study that the increase of control time resolution can limit performance of feedback control. Although the higher sampling and updating rate is known to be beneficial in control performance, the result implies that there can be some optimal control time step, which achieves sufficient bandwidth of the control system and favorable locations of NMP zeros at the same time.

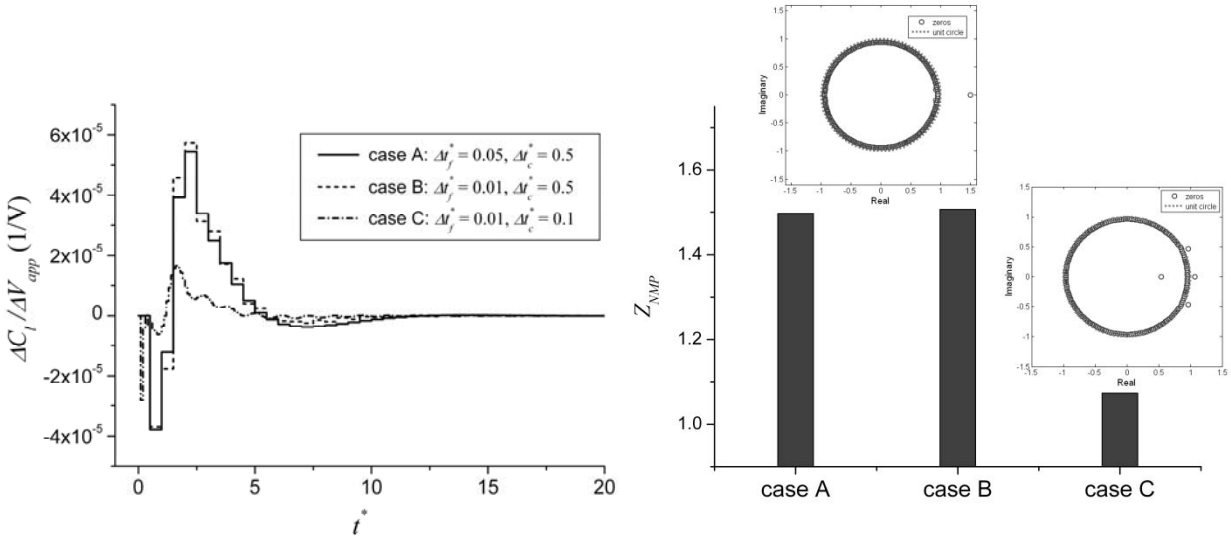

a) **b)**

Figure 12 Flow and control time resolutions and system parameters for lift (Re = 1000, α = 15°, $V_{app,0}$ = 1 kV, ΔV_{app} = 1 kV): a) impulse responses with different time resolutions; b) estimated NMP zeros and their locations in the complex domain.

The conditions, selected parameters, and key observations in this study are summarized in Table 1.

Table 1 Summary of the results.

Conditions / Issues	Reynolds number: Re = 300, 1000	Aspect ratio: AR = 4, 8, ∞	Actuation location: x_{act}/c = 0.05 ~ 0.7	Nominal voltage: $V_{app,0}$ = 1, 2 kV	Impulse or step amplitude: ΔV_{app} = 0.1 ~ 5 kV	Control time resolution: Δt_c^* = 0.1, 0.5
Order or the linearized transfer function	3~6 (delay is 1).					For Δt_c^* = 0.1, system order is 10 (delay is 1).
First nonzero Markov parameter(H_1) and real NMP zero(z_{NMP}) for lift	$\|H_1\|$ and z_{NMP} increase as Re increases.	z_{NMP} increases as AR increases.	z_{NMP} increases as actuation location moves downstream.	Not sensitive.	$\|H_1\|$ and z_{NMP} increase as step amplitude increases. Asymmetry in amplitude sign.	z_{NMP} decreases as time resolution increases.
Steady-state aerodynamic forces	Control authority on lift grows as Re increases. Penalty on drag decays as Re increases.	Control authority on lift grows as AR increases. Penalty on drag decays as AR increases.	Control authority on lift grows as actuation moves to downstream. Drag increase: no clear trend for Re = 300.	Not relevant.		
Dynamic aerodynamic force: lift	For higher Re, undershoot is larger but the steady-state lift increase is more substantial, resulting in decrease of the relative undershoot.	The relative undershoot decreases as the actuator moves to downstream and AR increases.		Not sensitive.	Steady-state lift increases faster than undershoot as step amplitude increases, resulting in smaller relative undershoot.	For higher time resolution, undershoot is larger, NMP zero is smaller.
Feedback performance	At a higher Reynolds number both lift and drag fluctuations can be suppressed at certain disturbance frequencies.	Controllable disturbance magnitudes are limited by the reduced control authority for a lower AR.	Only for 0.2.	Not sensitive but the lower voltage bound is limited by the breakdown voltage.	The NMP zero drift can limit the disturbance magnitude that can be suppressed.	Higher time resolution incorporates NMP zeros close to the unit circle. Lower time resolution causes higher steady-state error due to unresolved fluctuations.

V. Summary and Conclusions

In this study, the unsteady force evolutions on finite and infinite wings with the SD7003 airfoil geometry at Reynolds numbers between 300 and 1000 are stabilized by feedback control with the retrospective cost adaptive control (RCAC) algorithm using a dielectric barrier discharge (DBD) actuator. The flow unsteadiness caused by unsteady vertical flow speed induces unsteady aerodynamic forces, which can be coupled with the unstable vortex evolutions at a high angle of attack.

The regulated pressure field, especially intensified pressure and suction peaks around the DBD actuator, is shown as the main disturbance rejection mechanism. The open-loop actuation increases the steady-state lift by intensifying the suction peak and recovering the pressure loss in the separated flow with the penalty of the increased steady-state drag due to the increased friction drag. The closed-loop actuation, on the other hand, can suppress the fluctuations of lift and drag at the same time for the disturbance period of $T^* = 10$.

In most cases, the linearized transfer function of the flow-actuator system at $Re = 300 \sim 1000$ is nonminimum-phase for lift with a real NMP zero and has undershoot in response to voltage increase, whereas no real NMP zero and undershoot for drag. For modest free-stream fluctuations, the first nonzero Markov parameter and real NMP zero estimates are sufficient for the adaptive controller to stabilize lift fluctuations.

However, the real NMP zero and first nonzero Markov parameter are subject to geometric, flow and actuation conditions, and control time resolution: The more upstream actuation, lower wing aspect ratio and lower Reynolds number results in the smaller NMP zero. The lower vertical free-stream speed and smaller voltage variation induces the smaller NMP zero. The higher vertical free-stream speed, Reynolds number and voltage increment results in the larger absolute value of the first nonzero Markov parameter. The higher sampling rate decreases the magnitude of NMP zeros. Specifically, initial undershoot and steady-state lift in response to step actuation for different conditions are related to the NMP zero drift.

The NMP zero drifting, especially approaching to 1, which occurs under aforementioned conditions, can limit the control performance, implying that the trends can be used to optimize geometric and operational conditions of the DBD actuator to enhance control performance. Further study on the parametric drift can also enable the controller to achieve control goals under higher flow unsteadiness.

Acknowledgements

The present work is supported by the Air Force Research Laboratory, under a collaborative center agreement.

References

[1]Mueller, T. J., and DeLaurier, J. D., "Aerodynamics of small vehicles," *Ann. Rev. Fluid Mech.*, Vol. 35, 2003, pp. 89-111.

[2]Lissaman, P. B. S., "Low-Reynolds-number airfoils," *Ann. Rev. Fluid Mech.*, Vol. 15, 1983, pp. 223-239.

[3]Shyy, W., Berg, M., and Ljungqvist, D., "Flapping and flexible wings for biological and micro air vehicles," *Prog. Aero. Sci.*, Vol. 35, 1999, pp. 455-505.

[4]Shyy, W., Lian, Y., Tang, J., Viieru, D., and Liu, H., *Aerodynamics of Low Reynolds Number Flyers*, New York, Cambridge Univ. Press, 2008.

[5]Roth, J. R., Sherman, D. M., and Wilkinson, S. P., "Boundary layer flow control with a one atmosphere uniform glow discharge surface plasma," *AIAA Journal*, Vol. AIAA 98-0328, 1998.

[6]Moreau, E., "Airflow control by non-thermal plasma actuators," *J. Phys. D: Appl. Phys.*, Vol. 40, 2007, pp. 605-636.

[7]Taira, K., and Colonius, T., "Effect of tip vortices in low-Reynolds-number poststall flow control," *AIAA Journal*, Vol. 47, No. 3, 2009, pp. 749-756.

[8]Ahuja, S., and Rowley, C. W., "Low-dimensional models for feedback stabilization of unstable steady states," *46th AIAA Aerospace Sciences Meeting and Exhibit*, Reno, NV, 7-10 January, 2008, AIAA 2008-553.

[9]Muse, J. A., Tchieu, A. A., Kutay, A. T., Chandramohan, R., Calise, A. J., and Leonard, A., "Vortex model based adaptive flight control using synthetic jets," *AIAA Guidance, Navigation, and Control Conference*, Chicago, IL, 10-13 August, 2009, AIAA 2009-5761.

[10]Fledderjohn, M., Cho, Y.-C., Hoagg, J. B., Santillo, M., Shyy, W., and Bernstein, D. S., "Retrospective cost adaptive flow control using a dielectric barrier discharge actuator," *AIAA Guidance, Navigation, and Control Conference*, Chicago, Illinois, 10-13 August, 2009, AIAA 2009-5857.

[11]Cowan, T., Arena, A., and Gupta, K., "Development of a discrete-time aerodynamic model for CFD-based aeroelastic analysis," *37th AIAA Aerospace Sciences Meeting and Exhibit*, Reno, NV, 11-14 January, 1999, AIAA 99-0765.

[12]Lum, K.-Y., and Lai, K. L., "Identification of Hammerstein model for wing flutter analysis using CFD data and correlation method," *2010 American Control Conference*, (to be published).

[13]Rojas, C. R., Hjalmarsson, H., Gerencser, L., and Martensson, J., "Consistent estimation of real NMP zeros in stable LTI systems of arbitrary complexity," *15th IFAC Symposium on System Identification*, Saint-Malo, France, July 6-8, 2009.

[14]Holt, B. R., and Morari, M., "Design of resilient processing plants - VI. The effect of right-half-plane zeros on dynamic resilience," *Chemical Engineering Science*, Vol. 40, No. 1, 1985, pp. 59-74.

[15]Skogestad, S., and Postlethwaite, I., *Multivariable Feedback Control: Analysis and Design*, New York, John Wiley & Sons, 1996.

[16]Kim, J., and Bewley, T. R., "A linear systems approach to flow control," *Ann. Rev. Fluid Mech.*, Vol. 39, 2007, pp. 383-417.

[17]Rewienski, M., and White, J., "A trajectory piecewise-linear approach to model order reduction and fast simulation of nonlinear circuits and micromachined devices," *IEEE Transactions on Computer-Aided Design of Integrated Circuits and Systems*, Vol. 22, No. 2, 2003, pp. 155-170.

[18]Kamakoti, R., Thakur, S., Wright, J., and Shyy, W., "Validation of a new parallel all-speed CFD code in a rule-based framework for multidisciplinary applications," *36th AIAA Fluid Dynamics Conference and Exhibit*, San Francisco, CA, 5-8 June, 2006, AIAA 2006-3063.

[19]Shyy, W., Jayaraman, B., and Andersson, A., "Modeling of glow discharge-induced fluid dynamics," *J. Appl. Phys.*, Vol. 92, No. 11, 2002, pp. 6434-6443.

[20]Jayaraman, B., Cho, Y.-C., and Shyy, W., "Modeling of dielectric barrier discharge plasma actuator," *J. Appl. Phys.*, Vol. 103, 053304, 2008.

[21]Grundmann, S., Klumpp, S., and Tropea, C. "Experimental and numerical investigations of boundary-layer influence using plasma-actuators," *Active Flow Control, NNFM 95*. Springer, New York, 2007, pp. 56-68.

[22]Glauert, M. B., "The wall jet," *J. Fluid Mech.*, Vol. 1, No. 6, 1956, pp. 625-643.

[23]Hoagg, J. B., Santillo, M. A., and Bernstein, D. S., "Discrete-time adaptive command following and disturbance rejection with unknown exogeneous dynamics," *IEEE Transactions on Automatic Control*, Vol. 53, No. 4, 2008, pp. 912-928.

[24]Santillo, M. A., and Bernstein, D. S., "Adaptive control based on retrospective cost optimization," *Journal of Guidance, Control, and Dynamics*, Vol. 33, No. 2, 2010, pp. 289-304, DOI: 10.2514/1.46741.

[25]Rosenbrock, H. H., *State-space and Multivariable Theory*, London, Nelson, 1970.

[26]Stewart, J., and Davison, D. E., "On overshoot and nonminimum phase zeros," *IEEE Transactions on Automatic Control*, Vol. 51, No. 8, 2006, pp. 1378-1382.

[27]Lau, K., Middleton, R. H., and Braslavsky, J. H., "Undershoot and settling time tradeoffs for nonminimum phase systems," *IEEE Transactions on Automatic Control*, Vol. 48, No. 8, 2003, pp. 1389-1393.

[28]Ragazzini, J. R., and Franklin, G. F., *Sampled-data Control Systems*, New York, McGraw-Hill, Inc., 1958.